Applied Physics Letters ARTICLE scitation.org/journal/apl

Fast and efficient germanium quantum dot photodetector with an ultrathin active layer

Cite as: Appl. Phys. Lett. **119**, 221108 (2021); doi: 10.1063/5.0073355
Submitted: 29 September 2021 · Accepted: 17 November 2021 ·
Published Online: 1 December 2021

S. Shi,[1,a)] D. Pacifici,[1,2] and A. Zaslavsky[1,2]

AFFILIATIONS

[1]School of Engineering, Brown University, Providence, Rhode Island 02912, USA
[2]Department of Physics, Brown University, Providence, Rhode Island 02912, USA

[a)]Author to whom correspondence should be addressed: sue_shi@brown.edu

ABSTRACT

An ultrathin layer (13 nm) of germanium (Ge) quantum dots embedded in a SiO_2 matrix was deposited on a Ge substrate for photodetection in both the visible and near-infrared (IR). Operated at T = 150 K, the device exhibits higher than 10^5% internal quantum efficiency (IQE) at a reverse bias of −1.3 V under low light conditions (<30 nW) at both $\lambda = 640$ and 1550 nm. The transient response of 640 nm pulses stays below 15 ns for both rise and fall times; the IR response is only slightly slower. Our work demonstrates a high-performance broadband photodetector with high IQE and fast response in a simple silicon technology-compatible device structure.

Broadband photodetectors (PDs) in the visible and near-infrared (IR) offer a wide range of applications in optical imaging, sensing, and communications. A variety of materials, structures, and techniques have been explored for visible and near-IR photodetection.[1–17] Of these structures, Ge quantum dots (QDs) are particularly interesting given their spectral tunability and relative ease of integration into standard CMOS processing technology.[8,18–20] High-performance photodetectors based on this structure have been previously reported generally with impressive responsivity and internal quantum efficiency (IQE) but with slow response speed (especially in the near-IR).[8,21–24] In particular, Siontas *et al.*[8] demonstrated a Ge QD based photodetector on a Ge substrate with broadband detection and high IQE of up to 1000% at T = 100 K for 10 nW incident light at 1550 nm; however, the frequency response was limited to 60 kHz at best. We have recently reported a Si-substrate-based Ge QD PD for visible light detection with an improved response speed by thinning the active layer.[24] Here, we report a Ge QD PD fabricated on the Ge substrate, employing a ∼13 nm ultrathin active layer (W_{QD}) to improve the response speed in the near-IR. This is the thinnest possible active layer W_{QD} set by our QD diameters, which range from approximately 3 to 8 nm. Reducing the active layer thickness to such an ultrathin regime produces a high dark current at or close to room temperature; however, when cooled to temperatures achievable with Peltier cooling, our PDs simultaneously exhibit high efficiency and fast response speed in both the visible and near-IR. Aside from these improved figures of merit achieved by employing an ultrathin active layer, our work also sheds light on the thickness dependence of response speed in Ge QD PDs.

The detailed fabrication method has been previously reported,[24] except in this case we used a *n*-type Ge substrate (100) with 2.5–2.7 Ω cm resistivity. Here, we briefly summarize the fabrication process: Ge and SiO_2 were co-sputtered onto the *n*-type Ge substrate heated to 400 °C. The coated substrate was then annealed at 500 °C in N_2 for 30 min. The resulting thickness of the Ge:SiO_2 layer was verified with ellipsometry to be ∼13 nm. Optical lithography (Heidelberg MLA 150) was then used to define 0.5 × 0.5 mm^2 active areas onto which a 70 nm-thick ITO film was sputtered at room temperature to serve as the transparent top electrode, followed by a one-hour liftoff with Remover PG. The schematic of our device structure and a transmission electron microscopy (TEM) image of the active layer with visible lattice fringes of Ge quantum dots embedded in the SiO_2 matrix are shown in Fig. 1. Detailed TEM and x-ray diffraction analyses of the Ge-embedded SiO_2 matrix fabricated with the same or similar methods have been previously reported.[25,26] An indium back contact was added to the device before it was placed into a closed cycle cryostat (Advanced Research Systems) for temperature-controlled characterization.

The illumination source for both continuous wave (CW) and pulsed excitation was a supercontinuum laser (SuperK EXTREME, NKT Photonics) with a $\lambda = 400$–2400 nm spectral range and a

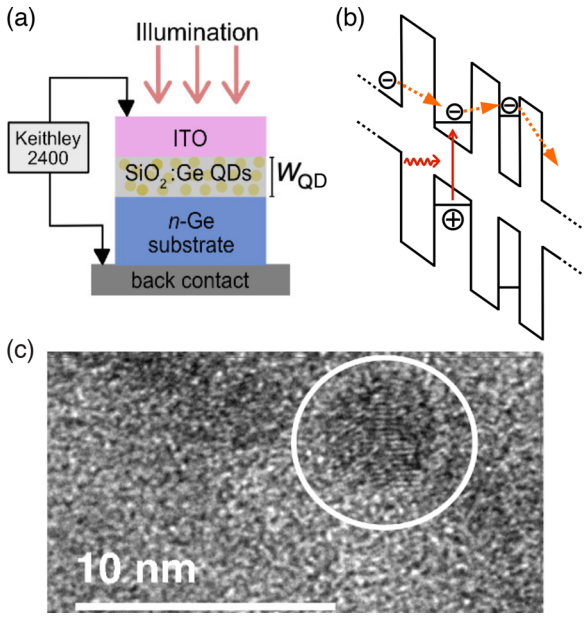

FIG. 1. (a) Schematic of our device consisting of an ITO electrode and an active layer with quantum dots on top of a *n*-Ge substrate. (b) Schematic illustration of the phonon-assisted tunneling process (indicated by orange dotted arrows) between neighboring QDs in an oxide matrix (represented by quantum wells of different sizes and energy levels). After a photon absorption (shown in red) takes place, either in a QD or in the substrate, electrons can hop between different QD energy levels (within the order of kT) by absorbing or emitting phonons. (c) A bright-field plan-view TEM micrograph of the Ge QDs taken with the JEOL 2100F at 200 kV at normal incidence. Lattice fringes of a quantum dot can be seen within the white circle.

variable repetition rate. The output of the laser was sent through a neutral density filter wheel, followed by a wavelength filter. The beam was then coupled into and decoupled from a single- (for visible illumination) or multi-mode (for IR) optical fiber (Thorlabs, Inc.), followed by a collimating lens and a density filter wheel before passing through the cryostat window and reaching the device. For CW excitation at 640 and 1550 nm, the repetition rate of the laser was set to 78 MHz, and bandpass filters (Thorlabs, Inc.) with the respective center wavelengths and FWHM $= 12 \pm 2.4$ nm were used. Data taken in the dark and under CW illumination were acquired using a Keithley 2400 source meter connected to the cryostat via coaxial cables. To probe the transient response of the device in the visible spectrum, a nanosecond pulsed laser diode system with $\lambda = 640$ nm (Thorlabs, Inc.) was set to the shortest 4.5 ns pulse width and triggered by a 1 kHz square wave. The laser beam was sent to the density filter wheel directly before entering the cryostat. The transient response in the IR was probed by the aforementioned supercontinuum laser but with a 7.8 MHz repetition rate. The beam path was the same as described for the CW characterization, except a 1400 nm longpass filter (Thorlabs, Inc.) was used instead of a bandpass filter. The readout circuit for transient characterization consisted of a voltage source (Keithley 230) biasing the device in the cryostat with the photocurrent signal read off a 100 Ω series resistor with a 200 MHz oscilloscope (Tektronix, Inc.).

The *I–V* characteristics of the device in the dark depend on the operating temperature and are shown in Fig. 2(a) from T = 77 to 300 K and from −2 to 1 V applied bias. The current limit was set to 1 mA to protect the device. At room temperature, the dark current of the PD exceeds the chosen current limit at low reverse biases due to the combination of high carrier concentrations in the Ge substrate and the thinness of the active layer, which becomes susceptible to high leakage currents compared to devices with thicker active layers or devices on silicon substrates. The dark current decreases with decreasing operating temperature and lower reverse bias, which can be attributed to a reduction in phonon-assisted tunneling and tunneling pathways within the oxide matrix, respectively. At a low operating voltage, the reverse-bias dark current can be significantly reduced by cooling the device to 100 K, while further cooling offers marginal improvement in dark current suppression. This is because the main carrier transport process is phonon-assisted tunneling between QDs in the SiO_2 matrix, as shown in Fig. 1(b). Phonons enable carrier hopping between levels that lie within an energy range of the order of kT, where k is

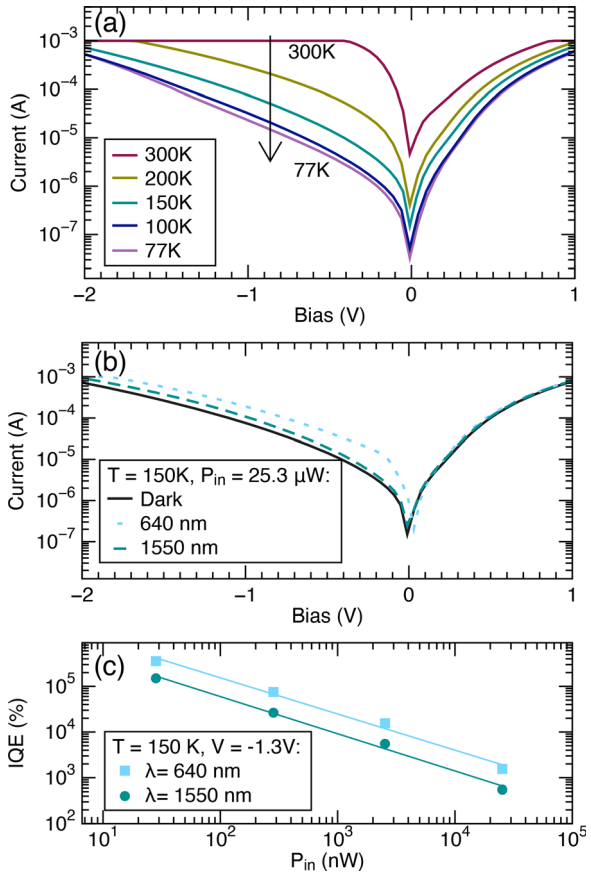

FIG. 2. (a) *I–V* curves of the Ge QD PD taken in the dark at various operating temperatures between 300 and 77 K with the current magnitude decreasing with temperature as illustrated by the arrow direction. (b) *I–V* curves of the Ge QD PD taken in the dark and under 640 and 1550 nm CW illumination at T = 150 K and at $P_{in} = 25.3\ \mu$W. (c) Calculated IQE as a function of P_{in} for CW illumination at $\lambda = 640$ and 1550 nm and at T = 150 K and an applied bias of −1.3 V. The lines are extrapolated from the data and serve as a visual guide.

Boltzmann's constant. As T is reduced, phonon absorption is suppressed, slowing the tunneling process. It is also possible for carriers to tunnel into surface states, which may become filled and, thus, neutralized at low T. We chose to investigate the incident power (P_{in}) dependence of the I–V characteristics at T = 150 K, as it is achievable by Peltier cooling,[27] making the device more technologically practical. The I–V curves for CW $\lambda = 640$ and 1550 nm at $P_{in} = 25.3\,\mu$W are plotted in Fig. 2(b). For both incident wavelengths, there is significant photocurrent under low reverse bias with the device's photoresponse to $\lambda = 640$ nm being stronger than to $\lambda = 1550$ nm. The IQEs of the device were calculated using Eq. (1) for a range of incident power values

$$\mathrm{IQE}(\lambda) = \frac{hc}{\lambda q(1 - R(\lambda))} \frac{I_{\mathrm{light}}(\lambda) - I_{\mathrm{dark}}}{P_{\mathrm{in}}}. \quad (1)$$

The results are plotted in Fig. 2(c) for T = 150 K at −1.3 V applied bias. The IQEs of the device in response to $\lambda = 640$ nm are higher than those to $\lambda = 1550$ nm and decrease with increasing incident power at both wavelengths. The higher IQE at 640 nm compared to 1550 nm can be attributed to the larger absorption coefficient and shorter penetration depth of 640 nm light in Ge, which allows more carriers in the substrate to be absorbed within a diffusion length of the QD-containing active region.[28] The decrease in the IQE with increasing incident power has been reported previously for this type of PD and was attributed to a sub-linear photocurrent growth across the incident power range due to saturation of available tunneling paths within the QD matrix.[8] The high IQE is attributable to a previously proposed hopping transport mechanism for devices based on this structure, where the heavier holes move much more slowly than the electrons and can be considered dynamically trapped in Ge QDs within the oxide matrix, resulting in a net positive charge build up that facilitates electron injection and flow through the QD active region to maintain charge neutrality, see Fig. 1(b).[8,26]

We probed the transient response of the Ge QD PD in both the visible and the IR from 77 to 200 K. (At 300 K, the photocurrent is swamped by the dark current.) The source for visible transient characterization at $\lambda = 640$ nm has a pulse width of 4.5 ns and an incident power of 3.8 mW with the pulse shape shown in the inset of Fig. 3(a). The response of the readout circuit is also shown in Fig. 3(a) with a fast transient main peak followed by ringing. We define the rise and fall times as the time it takes to rise to $1 - 1/e$ and fall to $1/e$ of the peak value, respectively. The rise and fall times at a fixed reverse bias of −1 V for a range of operating temperatures are plotted in Fig. 3(b). For all tested temperatures, the rise times stay under 10 ns, and the fall times under 15 ns with the response times staying relatively constant for all temperatures. We also measured the rise and fall times for various values of the reverse bias from 0 to −4 V and observed no significant bias dependence (not shown).

The IR transient response was characterized with the supercontinuum laser ($\lambda = 400$–2400 nm spectral range) and a 1400 nm long-pass filter. The effective characterized spectrum is from 1400 to 2400 nm, although the Ge substrate becomes transparent above 1850 nm. The repetition rate of the laser output was 7.8 MHz. Figure 4(a) shows the supercontinuum laser pulses (solid line) together with the PD circuit response (solid line with circles) at T = 150 K and V = −1 V. The slight phase shift between laser pulses and the circuit response may be the result of cabling from the laser to the oscilloscope.

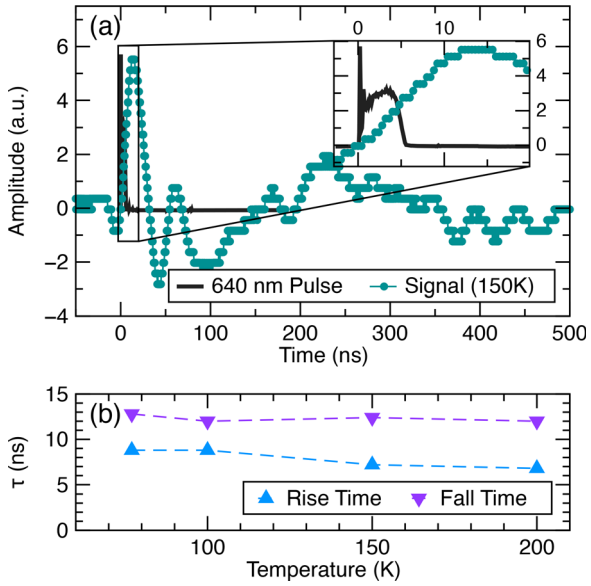

FIG. 3. (a) Transient response to a $\lambda = 640$ nm 4.5 ns pulse at T = 150 K, V = −1 V, and $P_{in} = 3.8$ mW. The inset magnifies the 4.5 ns pulse and the initial rise of the response signal. (b) Rise and fall times of the readout circuit to the 4.5 ns pulse at $\lambda = 640$ nm for various temperatures at V = −1 V.

The rise and fall times calculated with the aforementioned definitions are shown in Fig. 4(b) for a range of operating temperatures from 77 to 200 K. The response speeds in the IR are slightly slower than at 640 nm, which can be explained by the longer penetration depth of IR light in Ge. Carriers generated by an IR source are deeper in the substrate and take longer to travel to the QD-containing matrix, which

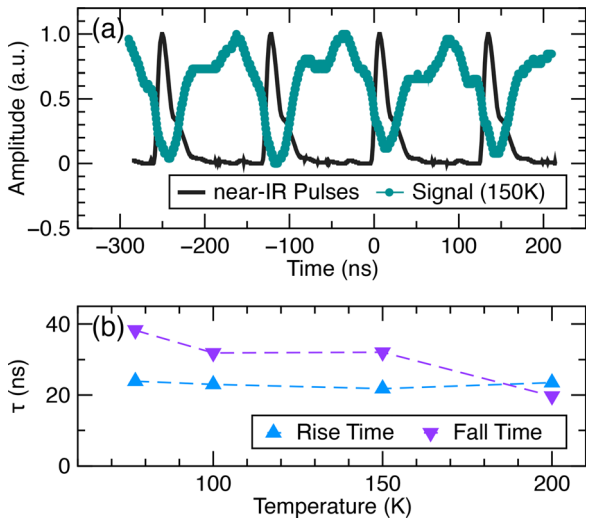

FIG. 4. (a) Transient response to a 7.8 MHz pulse train in the near-IR with 1400 nm $\leq \lambda \leq$ 2400 nm at T = 150 K and V = −1 V. (b) Rise and fall times of the readout circuit to the 7.8 MHz near-IR pulse train at V = −1 V reverse bias as a function of T in the 77–200 K range.

delays the transient response. Again, there does not appear to be any clear dependence of the response speed on either the operating temperature or the applied bias.

Previous work on this device structure has postulated that an improvement in the response speed can be achieved by thinning the active layer thickness and decreasing the device area, which could lower the RC circuit time constant via minimizing the parasitic resistance.[8,29] Our results show that we indeed achieved a faster response speed in both the visible and IR, while also improving the IQE. Since most of the light absorption occurs in the *n*-Ge substrate while the active layer amplifies the photocurrent with the aforementioned hopping transport mechanism, a thinner W_{QD} does not necessarily harm the IQE; in fact, the opposite may be true, as the reduction in the active layer thickness may yield devices with fewer defects.

In terms of the response speed's dependence on the active layer thickness, our results show partial agreement with the previous work. While we do observe an increased response speed with an ultrathin W_{QD}, our results do not support the previous claim that the fall time scales quadratically with $1/W_{QD}$, as proposed by Liu *et al.* in 2012 for devices with $W_{QD} = 60$–200 nm.[29] The $(W_{QD})^{-2}$ relationship may hold for devices with thicker active layers, in which the transport time is limited by diffusive inter-QD hopping through a thick W_{QD}, but a different mechanism could determine the response speed in the ultrathin W_{QD} regime. Indirect evidence for this can be seen in Figs. 3(b) and 4(b), which both show that the response speed does not depend strongly on the operating temperature. In previous studies, where the transient transport mechanism was dominated by charge hopping through many QDs, decreasing the operating temperature slowed the response speed, since the charge hopping time between dots was postulated to increase due to reduced phonon assistance.[8] Further study is needed to understand the dominant speed-limiting factor in ultrathin devices, where transport through the active layer may involve only 1–2 QDs. One possible candidate is the carrier lifetime in the QDs, which could determine the fall time of the photocurrent signal.

Table I shows the figures of merit for recently reported Ge or SiGe QD PDs characterized at or near the telecommunication wavelength. The characterization conditions were not identical, but we have selected the best reported values in each case. It is evident that our device with the ultrathin active layer can reach impressive responsivity and IQE while keeping the response speed in the ~10 ns range. There are also other reports of near–IR Ge QD PDs measured at shorter wavelengths with much lower efficiencies.[20,30]

In summary, we report an ultrathin active layer device with Ge QDs embedded in an oxide matrix on the *n*-Ge substrate for visible and near-IR photodetection. This is the thinnest active layer reported so far for such devices and shows a record IQE of up to $\sim 3 \times 10^5$% at $\lambda = 640$ nm and 10^5% at $\lambda = 1550$ nm with less than 30 nW incident power at T = 150 K, making them suitable for high-efficiency low-light detection. While the IQE decreases with increasing incident power, the values consistently exceed 100% across the measured incident power range from ~30 nW to 30 μW. When characterizing the transient response of this photodetector at a small reverse bias of −1 V, we achieved rise and fall times below 15 and 10 ns, respectively, for operating temperatures from 77 to 200 K, in the visible, and below 40 and 25 ns in the near-IR. Unlike the previous work on Ge QD-based devices with thicker active regions, our results indicate that the hopping conduction may not be the limiting mechanism for device speed. Our work demonstrates that extremely high IQE and nanosecond range response speed can be simultaneously achieved in Ge QD-based photodetectors that operate at low voltage, practical temperatures, and can, in principle, be integrated with silicon technology.

TABLE I. Near-telecom ($\lambda = 1400$–1630 nm) figures of merit of Ge or SiGe QD PDs.

Paper	Responsivity	IQE	Speed
Liu *et al.*[31]	9.7 A/W	···	40 μs
Siontas *et al.*[8]	···	1000%	5.83 μs
Stavrache *et al.*[14]	9.35 A/W	···	···
This work	470 A/W	1.5×10^5 %	22 ns

This project on Ge QD PDs at Brown University was originally funded by NSF via Award No. DMR-1203186; we also acknowledge the maskless lithography tool funded by NSF MRI award through No. DMR-1827453. S. Shi is a recipient of the Brown University Presidential Fellowship. Additionally, the authors gratefully acknowledge technical support by A. McCormick and M. Jibitsky.

AUTHOR DECLARATIONS

Conflict of Interest

The authors have no conflicts to disclose.

DATA AVAILABILITY

The data that support the findings of this study are available on request from the corresponding author.

REFERENCES

[1]C.-H. Liu, Y.-C. Chang, T. B. Norris, and Z. Zhong, "Graphene photodetectors with ultra-broadband and high responsivity at room temperature," Nat. Nanotechnol. **9**, 273–278 (2014).
[2]H. Qiao, J. Yuan, Z. Xu, C. Chen, S. Lin, Y. Wang, J. Song, Y. Liu, Q. Khan, H. Y. Hoh *et al.*, "Broadband photodetectors based on graphene–Bi_2Te_3 heterostructure," ACS Nano **9**, 1886–1894 (2015).
[3]Y. Liu, F. Wang, X. Wang, X. Wang, E. Flahaut, X. Liu, Y. Li, X. Wang, Y. Xu, Y. Shi *et al.*, "Planar carbon nanotube–graphene hybrid films for high-performance broadband photodetectors," Nat. Commun. **6**, 8589 (2015).
[4]L. Wang, J. Jie, Z. Shao, Q. Zhang, X. Zhang, Y. Wang, Z. Sun, and S.-T. Lee, "MoS_2/Si heterojunction with vertically standing layered structure for ultrafast, high-detectivity, self-driven visible-near infrared photodetectors," Adv. Funct. Mater. **25**, 2910–2919 (2015).
[5]H. Huang, J. Wang, W. Hu, L. Liao, P. Wang, X. Wang, F. Gong, Y. Chen, G. Wu, W. Luo *et al.*, "Highly sensitive visible to infrared $MoTe_2$ photodetectors enhanced by the photogating effect," Nanotechnology **27**, 445201 (2016).
[6]S. C. Dhanabalan, J. S. Ponraj, H. Zhang, and Q. Bao, "Present perspectives of broadband photodetectors based on nanobelts, nanoribbons, nanosheets and the emerging 2D materials," Nanoscale **8**, 6410–6434 (2016).
[7]S. Du, Z. Ni, X. Liu, H. Guo, A. Ali, Y. Xu, and X. Pi, "Graphene/silicon-quantum-dots/Si Schottky-PN cascade heterojunction for short-wavelength infrared photodetection," in *2017 IEEE International Electron Devices Meeting (IEDM)* (IEEE, 2017), p. 8-7.
[8]S. Siontas, H. Wang, D. Li, A. Zaslavsky, and D. Pacifici, "Broadband visible-to-telecom wavelength germanium quantum dot photodetectors," Appl. Phys. Lett. **113**, 181101 (2018).
[9]W. Hu, H. Cong, W. Huang, Y. Huang, L. Chen, A. Pan, and C. Xue, "Germanium/perovskite heterostructure for high-performance and broadband

photodetector from visible to infrared telecommunication band," Light **8**, 106 (2019).
[10]Q. Liang, Q. Wang, Q. Zhang, J. Wei, S. X. Lim, R. Zhu, J. Hu, W. Wei, C. Lee, C. Sow *et al.*, "High-performance, room temperature, ultra-broadband photodetectors based on air-stable $PdSe_2$," Adv. Mater. **31**, 1807609 (2019).
[11]M. Takiguchi, N. Takemura, K. Tateno, K. Nozaki, S. Sasaki, S. Sergent, E. Kuramochi, T. Wasawo, A. Yokoo, A. Shinya *et al.*, "All-optical InAsP/InP nanowire switches integrated in a Si photonic crystal," ACS Photonics **7**, 1016–1021 (2020).
[12]Z. Zhao, C. Xu, L. Niu, X. Zhang, and F. Zhang, "Recent progress on broadband organic photodetectors and their applications," Laser Photonics Rev. **14**, 2000262 (2020).
[13]C. Li, H. Wang, F. Wang, T. Li, M. Xu, H. Wang, Z. Wang, X. Zhan, W. Hu, and L. Shen, "Ultrafast and broadband photodetectors based on a perovskite/organic bulk heterojunction for large-dynamic-range imaging," Light **9**, 31 (2020).
[14]I. Stavarache, C. Logofatu, M. T. Sultan, A. Manolescu, H. G. Svavarsson, V. S. Teodorescu, and M. L. Ciurea, "SiGe nanocrystals in SiO_2 with high photosensitivity from visible to short-wave infrared," Sci. Rep. **10**, 3252 (2020).
[15]J. Yao and G. Yang, "2D material broadband photodetectors," Nanoscale **12**, 454–476 (2020).
[16]T. Zhu, Y. Yang, L. Zheng, L. Liu, M. L. Becker, and X. Gong, "Solution-processed flexible broadband photodetectors with solution-processed transparent polymeric electrode," Adv. Funct. Mater. **30**, 1909487 (2020).
[17]L.-C. Tien, Y.-C. Shih, C.-Y. Chen, Y.-T. Huang, and R.-S. Chen, "Broadband photodetectors based on layered 1D GaTe nanowires and 2D GaTe nanosheets," J. Alloys Compd. **876**, 160195 (2021).
[18]L. Rebohle, T. Gebel, J. V. Borany, W. Skorupa, M. Helm, D. Pacifici, G. Franzo, and F. Priolo, "Transient behavior of the strong violet electroluminescence of Ge-implanted SiO_2 layers," Appl. Phys. B **74**, 53–56 (2002).
[19]A. Yakimov, V. Kirienko, V. Armbrister, and A. Dvurechenskii, "Broadband Ge/SiGe quantum dot photodetector on pseudosubstrate," Nanoscale Res. Lett. **8**, 217 (2013).
[20]C. Chien, W. Lai, Y. Chang, C. Wang, M. Kuo, and P.-W. Li, "Size tunable Ge quantum dots for near-ultraviolet to near-infrared photosensing with high figures of merit," Nanoscale **6**, 5303–5308 (2014).
[21]P. Liu, S. Le, S. Lee, D. Paine, A. Zaslavsky, D. Pacifici, S. Cosentino, S. Mirabella, M. Miritello, I. Crupi *et al.*, "Fast, high-efficiency Germanium quantum dot photodetectors," in *2012 Lester Eastman Conference on High Performance Devices (LEC)* (IEEE, 2012), pp. 1–3.
[22]M.-H. Kuo, M.-C. Lee, H.-C. Lin, T. George, and P.-W. Li, "High photoresponsivity Ge-dot photoMOSFETs for low-power monolithically-integrated Si optical interconnects," Sci. Rep. **7**, 44402 (2017).
[23]I. Stavarache, V. S. Teodorescu, P. Prepelita, C. Logofatu, and M. L. Ciurea, "Ge nanoparticles in SiO_2 for near infrared photodetectors with high performance," Sci. Rep. **9**, 10286 (2019).
[24]S. Shi, A. Zaslavsky, and D. Pacifici, "High-performance germanium quantum dot photodetectors: Response to continuous wave and pulsed excitation," Appl. Phys. Lett. **117**, 251105 (2020).
[25]S. Cosentino, S. Mirabella, M. Miritello, G. Nicotra, R. L. Savio, F. Simone, C. Spinella, and A. Terrasi, "The role of the surfaces in the photon absorption in Ge nanoclusters embedded in silica," Nanoscale Res. Lett. **6**, 135 (2011).
[26]S. Cosentino, E. Barbagiovanni, I. Crupi, M. Miritello, G. Nicotra, C. Spinella, D. Pacifici, S. Mirabella, and A. Terrasi, "Size dependent light absorption modulation and enhanced carrier transport in germanium quantum dots devices," Sol. Energy Mater. Sol. Cells **135**, 22–28 (2015).
[27]M. Bommer, "InP/(Al, Ga) InP quantum dots on GaAs-and Si-substrates for single-photon generation at elevated temperatures," Ph.D. thesis (University of Stuttgart, 2013).
[28]Thorlabs, Inc., *Photodiode Rise Time Increases with Wavelength of Incident Light* (Thorlabs, Inc., 2020).
[29]P. Liu, S. Cosentino, S. T. Le, S. Lee, D. Paine, A. Zaslavsky, D. Pacifici, S. Mirabella, M. Miritello, I. Crupi *et al.*, "Transient photoresponse and incident power dependence of high-efficiency germanium quantum dot photodetectors," J. Appl. Phys. **112**, 083103 (2012).
[30]Y. Zhao, L. Li, S. Liu, J. Wang, J. Xu, Y. Shi, K. Chen, P. R. i Cabarrocas, and L. Yu, "Germanium quantum dot infrared photodetectors addressed by self-aligned silicon nanowire electrodes," Nanotechnology **31**, 145602 (2020).
[31]X. Liu, X. Ji, M. Liu, N. Liu, Z. Tao, Q. Dai, L. Wei, C. Li, X. Zhang, and B. Wang, "High-performance Ge quantum dot decorated graphene/zinc-oxide heterostructure infrared photodetector," ACS Appl. Mater. Interfaces **7**, 2452–2458 (2015).